Synthesis, structure and physical properties of luminescent Pr(III) *β*-diketonate complexes

V. M. Pereira[1], A. L. Costa[2], J. Feldl[1,3], T.M.R. Maria[2], J.S. Seixas de Melo[2], P. Martín-Ramos[1,4*], J. Martín-Gil[5] and M. Ramos Silva[1*]

[1] CFisUC, Department of Physics, University of Coimbra, Rua Larga, P-3004-516 Coimbra, Portugal. Phone: +351.239.410648; Fax: +351.239.829158. E-mail: manuela@pollux.fis.uc.pt.

[2] CQC, Department of Chemistry, University of Coimbra, Rua Larga, P-3004-535 Coimbra, Portugal.

[3] Fakultät für Physik, Ludwig-Maximilians-Universität, Schellingstrasse 4, 80799 München, Germany.

[4] Higher Polytechnic School of Huesca, University of Zaragoza, Carretera de Cuarte s/n, 22071 Huesca, Spain. Phone: +34 (974) 292668; Fax: +34 (974) 239302. E-mail: pmr@unizar.es.

[5] Advanced Materials Laboratory, ETSIIAA, Universidad de Valladolid, Avda. Madrid 44, 34004 Palencia, Spain.

Abstract

Near infrared lanthanide(III)-based light conversion molecular devices (LCMDs) are emerging as a promising class of materials for organic light-emitting diodes (OLEDs) in some niche technologies. Three of these molecular materials -two highly coordinated Pr^{3+} *β*-diketonate monomers and a dimer- are presented and their structure and properties are discussed. Particular emphasis is placed on the solid-to-solid transformation observed for the homodinuclear compound.

Keywords: beta-diketonate; dimer; luminescence; praseodymium; phase transition.

1. Introduction

Over the past decade, the research effort on organic light-emitting diodes (OLEDs) has been focused on devices which emit almost exclusively in the visible part of the electromagnetic spectrum (390 to 700 nm). More recently, there has been a growing interest in low-cost materials that emit in the near-infrared (NIR, 700 to 2500 nm), given their potential applications in optical communication networks, sensor technology, micro-circulatory blood flow imaging, photoplethysmography, photodynamic therapy or in the nanobiophotonics field [1].

Among these materials, lanthanide complexes (including Pr^{3+}) are particularly promising because they emit well-defined bright light in the near infrared region. The sensitization of the Ln(III) luminescence in the NIR region is, however, more difficult than in the visible one and deactivation of the excited states by the vibrations of the ligands and/or solvent molecules are much more rapid.

One way to overcome this problem is by coordinating the lanthanide ions with organic molecules specifically designed for this purpose, which can absorb the excitation energy efficiently and transfer it to the lanthanide ion (by *antenna effect*) and also minimize deleterious vibrations in the surroundings of the Ln^{3+} ion by resorting, for example, to halogenation or deuteration [2].

Photophysical studies on complexes of Pr^{3+} are relatively rare, in particular those involving time-resolved measurements, but solid acetate [3], pyrazolylborate [4,5], N-oxides [6,7], *m*-terphenyl-containing polydentate ligands [8], 4-Hydroxy-6-methylnicotinic acid [9], imines [10,11], amides [12,13] and *β*-diketonates [14-20] have been reported to be suitable sensitizers

for Pr^{3+}. Amongst these different ligands, β-diketonates would be the most popular choice, due to their commercial availability, their easy modification by substituents on the heterocycle ring, and the fact that the resulting complexes usually feature good thermal stability, good processability and thin-film forming properties, and reasonably well-balanced carrier transport properties, making them suitable –for example- as emissive layers in aforementioned OLEDs.

We hereby present a series of three Pr^{3+} coordination complexes in which the primary sensitizing ligand is a highly fluorinated β-diketonate (6,6,7,7,8,8,8-heptafluoro-2,2-dimethyl-3,5-octanedione, Hfod): a monomer in which methanol and water molecules enter in the first coordination environment, a homodinuclear complex in which the β-diketonate and a water molecule act as bridging ligands, and a second monomer in which a bulky N,N-donor (bathophenanthroline, bath) completes the first coordination sphere. These novel materials have been characterized by X-ray diffraction, Fourier transform infrared spectroscopy, thermogravimetric analysis, polarized light thermal microscopy, absorption and luminescence spectroscopy, and magnetic susceptibility measurements.

Particular emphasis will be placed on the thermal behavior of the dimer, $[Pr_2(fod)_6(H_2O)\cdot H_2O]$, for which a plastic phase has been identified. Crystal to plastic phase transitions are extremely rare in β-diketonate lanthanides complexes and still very uncommon in lanthanide complexes consisting of monomer or dimers (whereas such solid-to-solid phase transitions associated with hydration and re-hydration are more common in metal-organic frameworks (MOFs)).

2. Material and methods

2.1. *Materials and synthesis*

All reagents and solvents employed were commercially available and used as supplied, without further purification.

Very small crystals of the homodinuclear complex, hexa(6,6,7,7,8,8,8-heptafluoro-2,2-dimethyl-3,5-octanedionate)-di-praseodymium(III)-aqua hydrated, $[Pr_2(fod)_6(H_2O)\cdot(H_2O)]$, complex **1**, were found amongst the powder of the same compound sold by Fluka as tris(6,6,7,7,8,8,8-heptafluoro-2,2-dimethyl-3,5-octanedionate)praseodymium(III) [purum, CAS No. 17978-77-7]. An early study of structure of this compound was reported in 1971 by De Villers *et al*. [21].

Tris(6,6,7,7,8,8,8-heptafluoro-2,2-dimethyl-3,5-octanedionate)-praseodymium(III)-methanol-aqua, $[Pr(fod)_3(H_2O)(OHCH_3)]$ or complex **2**, was obtained by recrystallization of aforementioned commercial product in methanol.

Tris(6,6,7,7,8,8,8-heptafluoro-2,2-dimethyl-3,5-octanedionate)mono(bathophenanthroline) praseodymium(III), $[Pr(fod)_3(bath)]$ or complex **3**, was obtained by mixing of equimolar quantities tris(6,6,7,7,8,8,8-heptafluoro-2,2-dimethyl-3,5-octanedionate)praseodymium(III) (1.026 g, 1 mmol) and bathophenanthroline [4,7-diphenyl-1,10-phenanthroline 97%, CAS No. 1662-01-7, Sigma Aldrich] (0.332 g, 1 mmol) in methanol. The mixture was heated to 75 ºC and stirred overnight, then washed with dioxane, and finally dried in vacuum to give the product in 86% yield (based in Pr). Crystals suitable for X-ray analysis were obtained by slow evaporation of a methanol-dioxane solution at room temperature (RT).

2.2. *X-ray diffraction crystallographic analysis*

For the determination of the three crystal structures presented herein, single crystals were glued to glass fibres and mounted on a BruKer APEX II diffractometer. Diffraction data was collected at room temperature 293(2) K using graphite monochromated Mo-κα (λ=0.71073 Å) radiation. Absorption corrections were made using SADABS [22]. The structures were solved by direct methods using SHELXS-97 and refined anisotropically (non-H atoms, non-disordered atoms) by full matrix least-squares on F^2 using the SHELXL-97 program [23]. PLATON [24] was used for structure analysis and figure plotting.

For complex **1** the quality of diffraction data from a few tested crystals was poor. The crystal model showed signs of disorder and some alternative positions were found for terminal groups. Some terminal atoms were refined only isotropically and restraints to the refinement such as DFIX restraints were used. The bridging water H atoms were positioned to maximize H-bonds. The non-coordinating water molecule could not be located. Remaining H atoms were positioned using SHELXL-97 defaults.

For complex **2**, a good quality crystal was used. Some signs of disorder in the terminal groups of the β-diketonate chains could be seen. Water and hydroxyl H-atoms could be located on a Fourier difference map. Remaining H atoms were positioned using SHELXL-97 defaults.

For complex **3** the quality of diffraction data from a few tested crystals was poor. The crystal model showed signs of disorder and some alternative positions were found for terminal groups. Some terminal atoms were refined only isotropically and restraints to the refinement such as DFIX restraints were used.

2.3. *Physical measurements*

X-ray powder diffraction (XRPD) was performed with Cu-Kα1 (λ=1.540598 Å) radiation in the Debye-Scherrer geometry in an ENRAF-NONIUS FR590 powder diffractometer equipped with an INEL CPS120 detector. A small amount of powder of each sample was used to fill a capillary, which was kept rotating during data collection. The sample of complex **1** was cooled/heated by a nitrogen gas stream (Oxford Cryosystems, series 600) at an approximate rate of 6 °C/min in the -150 to 120°C range.

Infrared spectra of the compounds were obtained in pure powder form using a Thermo Nicolet 380 Fourier transform infrared spectroscopy (FT-IR) apparatus equipped with Smart Orbit Diamond Attenuated Total Reflection (ATR) system. The $[Pr_2(fod)_6(H_2O) \cdot H_2O]$ sample was studied both before and after the solid-to-solid transformation.

Differential scanning calorimetry (DSC) data were obtained on a Perkin Elmer DSC7 instrument, equipped with an intracooler cooling unit at -10 ℃ (ethylenglycol-water, 1:1 v/v, cooling mixture), with a heating rate β=10°C/min, under a N_2 purge, 20 mL/min. Samples were hermetically sealed in aluminium pans, and an empty pan was used as a reference. Temperature calibration was performed with high-grade standards, biphenyl (CRM LGC 2610) and indium (Perkin-Elmer, x=99.99%), which was also used for enthalpy calibration [25,26]. Thermogravimetric (TG) and differential thermal analyses (DTA) were carried out in an inert atmosphere with a Perkin Elmer simultaneous thermal analyzer STA6000, by heating the samples in a slow stream of N_2 (40 mL/min) from room temperature up to 300 ℃, with a heating rate of 10 ℃/min.

Polarized light thermal microscopy (PLTM) measurements were conducted on a DSC600 hot stage Linkam system, with a Leica DMRB microscope and a Sony CCD-IRIS/RGB video camera. The images were obtained by combined use of polarized light and wave compensators, using a 200× magnification. Real Time Video Measurement System software by Linkam was used for image analysis. A picture was taken every four seconds while ramping the temperature from 25 °C up to 200 °C at a 10 °C/min rate.

Magnetic properties of complex **1** were recorded with a QuantumDesign PPMS DynaCool using the Vibrating Sample Magnetometer option. The sample (m=1.65 mg) was inserted as a loose powder in the plastic sample holder. The susceptibility curve was measured under a constant field of 1000 Oe in the 1.8-312 K temperature range.

2.4. *Optical measurements*

Optical absorption and photoluminescence (PL) spectra of the materials were measured at room temperature. The 200-1400 nm range diffuse reflectance (DR) absorption spectra in powder form and the absorption spectra in cyclohexane were recorded on a Cary 5000 UV-Vis-NIR spectrophotometer. The solid-state photoluminescence spectra in the visible region and the

excitation spectra (monitoring the λ=469 nm emission in the 250-500 nm range) were recorded with a Horiba-Jobin-Ivon SPEX FluoroLog 3–22 spectrometer using an ozone-free 450 W Xenon lamp as the excitation source and a Hamamatsu R928 photomultiplier (200-950 nm range) detector, cooled with a Products for Research thermoelectric refrigerated chamber (model PC177CE005). The PL spectra in the NIR region were excited with a laser diode at 370 nm and collected with a 0.303 focal length Shamrock SR-303i spectrograph with an Andor Newton cooled Electron Multiplying CCD (EMCCD) camera. Lifetimes were measured by using a Tektronix (model 3840) oscilloscope. All spectra have been corrected by the spectral response of the experimental setups.

3. Results and discussion

3.1. *Structural description*

In the crystal structure of $[Pr_2(fod)_6(H_2O) \cdot H_2O]$, the lanthanide ions assemble in non-centrosymmetric dimers that crystallize in centrosymmetric unit cells of volume 8295 $Å^3$ (see Table 1).

Within the dimer, the lanthanide ions are 3.988 Å apart and are bridged by two carbonyl oxygen atoms and one water oxygen (Figure 1). Each Pr^{3+} is coordinated by 8 oxygen atoms in a distorted coordination polyhedra between a bicapped trigonal prism and a dodecahedron (see Table 2 for Pr…O distances). The $β$-diketonate chains show signs of positional disorder with the position of the F atoms poorly defined. The bridging water shares its H atoms with a $β$-diketonate oxygen atom and a fluorine atom from neighbouring molecules within the dimer (Table 3). The hydration water could not be located: in fact, the average structure do not allow voids (for a water molecule circa 40 $Å^3$ are needed). The hydration water molecules take advantage of the disorder in the chains conformation, which would statistically allow for their insertion in the crystal structure.
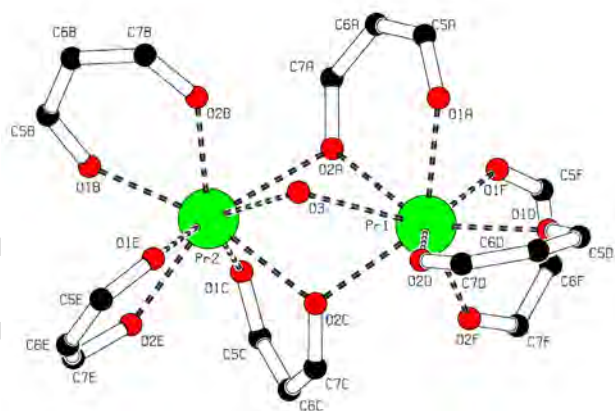

Figure 1. Molecular structure of $[Pr_2(fod)_6(H_2O) \cdot H_2O]$, where only the central $β$-diketonate moieties and the oxygen water are shown for clarity reasons.
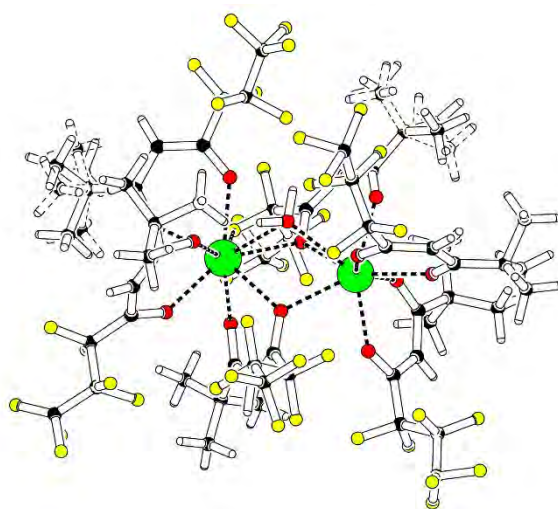
Figure 2. The molecular structure of $[Pr_2(fod)_6(H_2O)\cdot H_2O]$ compound. The Pr^{3+} ions are shown as large green spheres. The F atoms (*yellow*) and the $C(CH_3)_3$ groups (*black*) shown signs of positional disorder.

Table 1. Crystal data and structure refinement for the three Pr(III) complexes under study.

Complex	Complex **1** $[Pr_2(fod)_6(H_2O)\cdot H_2O]$	Complex **2** $[Pr(fod)_3(H_2O)(HOCH_3)]$	Complex **3** $[Pr(fod)_3(bath)]$
Empirical formula	$C_{60}H_{62}F_{42}O_{13}Pr_2$	$C_{31}H_{36}F_{21}O_8Pr$	$C_{54}H_{46}F_{21}N_2O_6Pr$
Formula weight	2070.92	1076.51	1358.84
Temperature (K)	293(3)	293(2)	293(2)
Wavelength (Å)	0.71073	0.71073	0.71073
Crystal system	Monoclinic	Triclinic	Triclinic
Space group	P 2_1/n	P -1	P -1
a (Å)	14.2109(11)	12.4133(3)	16.1777(5)
b (Å)	25.6139(19)	13.5781(3)	16.2920(5)
c (Å)	23.1839(14)	14.7950(3)	23.0562(6)
α (°)	90.00	63.3700(10)	84.1180(16)
β (°)	100.580(5)	88.4800(10)	82.4408(17)
γ (°)	90.00	76.8730(10)	87.9817(18)
Volume (Å³)	8295.4(10)	2162.77(8)	5990.9(3)
Z	4	2	4
Calculated density (g·cm⁻³)	1.658	1.653	1.507
Absorption coefficient (mm⁻¹)	1.307	1.260	0.926
$F(000)$	4088	1068	2720
θ range for data collection (°)	2.16-25.87	2.20-25.83	2.0-25.92
Index ranges	-17<*h*<17; -31<*k*<31; -28<*l*<28	-15<*h*<15; -16<*k*<16; -18<*l*<18	-19<*h*<19; -19<*k*<19; -28<*l*<28
Reflections collected	167849	38037	120156
Independent reflections	15927	8258	22461
Completeness to 2θ=51°	99.2%	98.9%	96.2%
Refinement method	Full matrix LS on F^2	Full matrix LS on F^2	Full matrix LS on F^2
Data/restrains/parameters	15927/108/975	8258/12/569	22461/125/1530
Goodness-of-fit on F^2	1.013	1.023	1.013
Final R indices [$I>2\sigma(I)$]	R=0.1108; wR=0.2581	R=0.0477; wR=0.1306	R=0.1075; wR=0.3063
R indices (all data)	R=0.3575; wR=0.3618	R=0.0594; wR=0.1423	R=0.2020; wR=0.3499
Largest diff. peak and hole	-1.360/1.428	-0.907/1.074	-1.273/1.429

Table 2. Pr-O distances for complex **1**.

Bond	Distance (Å)	Bond	Distance (Å)
Pr1–O1A	2.417(3)	Pr2–O1B	2.398(4)
Pr1–O2A	2.497(3)	Pr2–O2B	2.410(4)
Pr1–O1D	2.416(4)	Pr2–O1C	2.449(3)
Pr1–O2D	2.391(4)	Pr2–O2C	2.479(3)
Pr1–O1F	2.435(4)	Pr2–O1E	2.377(4)
Pr1–O2F	2.358(4)	Pr2–O2E	2.413(4)
Pr1–O2C	2.491(3)	Pr2–O2A	2.614(3)
Pr1–O3	2.738(3)	Pr2–O3	2.673(4)

Table 3. Hydrogen bonding geometry for complex **1**.

D-H..A	d(D-H)	d(H..A)	d(D..A)	∠DHA
O3-H3A..O1E	0.818	2.113	2.917	167.49
O3-H3B..F3B	0.935	2.169	3.082	164.97

Complex **2**, tris(6,6,7,7,8,8,8-heptafluoro-2,2-dimethyl-3,5-octanedionate)-aqua-methanol praseodymium(III), [Pr(fod)$_3$(H$_2$O)(HOCH$_3$)], crystallizes in a triclinic centrosymmetric unit cell. The molecules assemble in monomers with three β-diketonate ligands coordinating each lanthanide ion. Also playing a coordination role, there is one water molecule and a methanol molecule. The 8 oxygen atoms surrounding Pr^{3+} ion are disposed in a square-antiprismatic geometry with the lanthanide ion occupying roughly the centre of the polyhedron (Table 4). The water molecules bridge the monomers into dimers through hydrogen bonds (Table 5). Within the dimer, the Pr^{3+} ions are 5.872 Å apart.
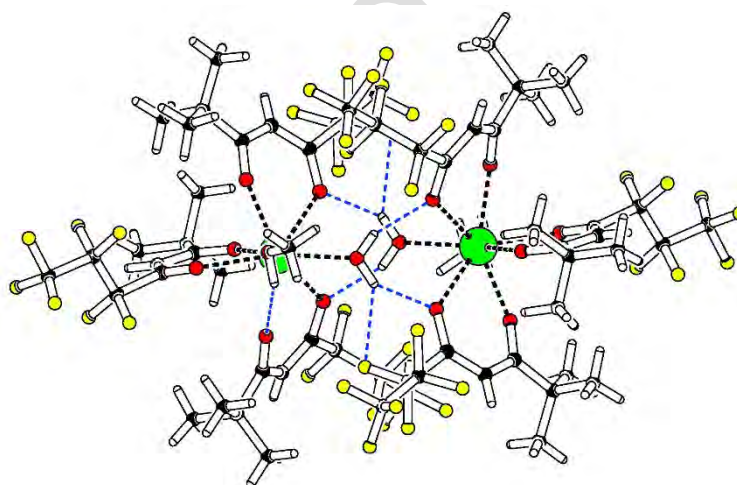
Figure 3. Structural diagram of complex **2**. Pr^{3+} ions are drawn as large green spheres. Coordination bonds are drawn as thick dashed lines. H-bonds are depicted as blue dashed lines.

Table 4. Pr-O distances for [Pr(fod)$_3$(H$_2$O)(HOCH$_3$)]

Bond	Distance (Å)	Bond	Distance (Å)
Pr1–O1A	2.421(2)	Pr1–O1C	2.362(2)
Pr1–O2A	2.468(2)	Pr1–O2C	2.438(3)
Pr1–O1B	2.414(3)	Pr1–O3	2.506(2)
Pr1–O2B	2.460(2)	Pr1–O4	2.522(3)

Table 5. Hydrogen bonding geometry for complex **2**.

D-H..A	d(D-H)	d(H..A)	d(D..A)	∠DHA
O3-H3A...O2A^i	0.84(5)	2.01(5)	2.796(3)	155(4)
O3-H3B...F2B^i	0.88(4)	2.43(4)	3.148(5)	140(4)
O3-H3B...O2B^i	0.88(4)	2.07(5)	2.831(3)	144(4)

i=-x,2-y,-z

Complex **3**, [Pr(fod)$_3$(bath)], crystallizes in a centrosymmetric triclinic unit cell with two monomers in the asymmetric unit cell (Figure 4, Table 1). Three fod ligands and one bathophenanthroline ligand coordinate the lanthanide ion in each monomer. The fluorinated chains of the fod ligands show positional disorder, with alternative chain conformations. The six O atoms and the two N atoms that coordinate the central Pr^{3+} ion provide a square anti-prismatic environment, with the lanthanide ion roughly at the centre of the prism. The antiprism has two nearly parallel top and bottom faces, which make an angle of 4.9(6)º and 3.1(5)º for monomer 1 and 2, respectively. Pr-O and Pr-N distances are summarized in Table 6. Pr^{3+} ions are very far apart and no interaction between them is expected (Pr1…Pr2 distance is over 10 Å). There is no conventional H-bonding joining the monomers.
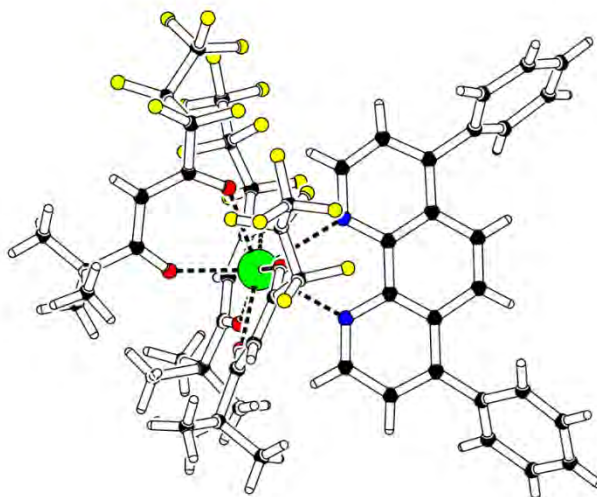
Figure 4. Molecular structure of [Pr(fod)$_3$(bath)] complex.

Table 6. Pr-O and Pr-N distances for [Pr(fod)$_3$(bath)]

Bond	Distance (Å)	Bond	Distance (Å)
Pr1–O1A	2.400(17)	Pr2–O7	2.420(17)
Pr1–O2A	2.416(19)	Pr2–O8	2.382(16)
Pr1–O1B	2.439(15)	Pr2–O9	2.430(18)
Pr1–O2B	2.372(19)	Pr2–O10	2.405(19)
Pr1–O1C	2.391(18)	Pr2–O11	2.420(19)
Pr1–O2C	2.405(18)	Pr2–O12	2.42(2)
Pr1–N1	2.691(19)	Pr2–N3	2.68(2)
Pr1–N2	2.675(18)	Pr2–N4	2.679(18)

All aforementioned complexes (**1**, **2** and **3**) crystallize in centrosymmetric space groups. Complexes **1** and **2** assemble in dimers, with a strong intra-dimeric bridge in **1** and a loose bridge in **2**. The insertion of bathophenathroline in the lanthanide coordination sphere, as it is the case in **3**, leads to the formation of isolated monomers. In **1**, the coordinating O atoms make the edges of

a distorted eight-vertex bisdisphenoid, while in **2** and **3** the coordinating O,N atoms define a distorted square-antiprism.

There are just a few other compounds described in literature, containing Pr^{3+}, β-diketonates and N,N-donors, equally aiming at efficient energy transfer from the ligands to the central lanthanide ion [17,18,27,28]. In such compounds, the Ln-O and Ln-N distances are similar to those reported herein.

3.2. *X-ray powder diffraction*

At room temperature, the powder diffractogram of complex **1** (see Figure 5, solid line) showed a perfect agreement with the simulated pattern from the single crystal data, thus excluding the presence of other phases or of other crystalline impurities. The low ratio of peak-to-background pointed to a low degree of crystallinity of the sample.

When the temperature was increased above 90ºC, a solid-to-solid transformation took place. The room temperature diffraction peaks disappeared and two new peaks appeared (see Figure 5, dashed and dotted lines). This transformation was irreversible: lowering the temperature down to -150ºC did not change the diffractogram. After waiting for a few days, keeping the sample at RT after having induced the transformation, the diffraction experiment was repeated yielding the same results.

The second phase still corresponded to a solid phase. The diffractogram was characteristic of a very symmetric arrangement of the dimers inside the crystal grains. In fact the two reflections could be indexed in a face centered cubic cell of dimensions a=20.962 Å (V=9210.8 Å^3). The volume per dimer (2302 Å^3) would be slightly higher than the original one (2073 Å^3).

The cubic periodicity should correspond to the periodicity of the position of the center of mass of the dimers. The precise orientation of the molecules in relation the center of mass would be lost and, in average, the dimer assembling would look like a nearly spherical cloud of atoms with the center of mass portraying a regular periodicity.

When the sample was heated above 100 ºC, it could be observed that, when touched with a spatula, the sample resembled a wax. This may indicate that at this temperature the dimers form a plastic phase.

For complexes **2** and **3**, the experimental powder diffractograms (not shown) were also in good agreement with the predicted powder patterns generated from single crystal data.
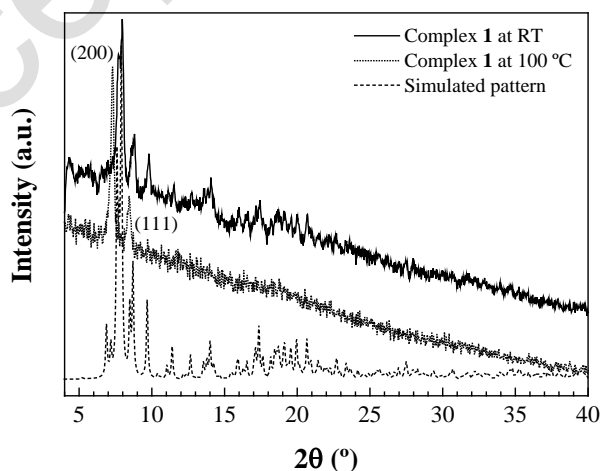

Figure 5. Evolution of the X-ray powder diffraction patterns of $[Pr_2(fod)_6(H_2O)\cdot H_2O]$ with temperature.

3.3. *Vibrational characterization*

The FT-IR absorption spectra for the complexes are shown in Figure 6. The presence of the fod ligand in the three complexes justifies that they share the absorbance bands attributed to this moiety in the literature [29]: 1581 cm^{-1} and 1508-1506 cm^{-1} (νC=C), 1466-1458 cm^{-1} (ν_{as}C-C=C-O) and 1344 cm^{-1} (ν_sC-C=C-O). They are shifted in comparison with those of the free ligand, suggesting that the fod β-diketonate ligand is coordinated to Pr^{3+} ions.

An important feature –provided that fod is a highly fluorinated ligand– is the occurrence of strong carbon–fluorine bands in the 1109 to 1277 cm^{-1} range, assigned to CF$_3$ as (C–F) stretching modes (*viz.*, νC-CF$_3$ at 1277 and 1221 cm^{-1}, ν_{as}CF$_3$ at ca. 1151 cm^{-1} and ν_sCF$_3$ at 1116-1109 cm^{-1}). In addition, the bands at around 527 and 466 cm^{-1} can be assigned to δCF$_3$ vibrations [30].

In [Pr$_2$(fod)$_6$(H$_2$O)·H$_2$O] complex, peaks at 1615 cm^{-1} and 1638 cm^{-1} are observed, which may be associated to O-H bending vibrations of the two different water molecules (bridging and solvated, respectively). Other vibration modes that can be ascribed to the bridging water molecule are: rocking (out-of-plane bending) at 809 cm^{-1}, wagging vibration at 664 cm^{-1}, and Pr-O vibration at 596 cm^{-1} [31].

In the [Pr(fod)$_3$(H$_2$O)(HOCH$_3$)], the broad band centered at 3396 cm^{-1} is caused by the O-H stretching vibration modes (those from of the coordinated water molecule appear at 3270 cm^{-1}). The deformation OH vibration of coordinated water and methanol can be found at 1615 cm^{-1} and 1482-1469 cm^{-1}, respectively [32].

In [Pr(fod)$_3$(bath)] complex, the absorption band characteristic of the bath diimide at 1428 cm^{-1} (ν_sC=N) and those at 939, 858 and 702 cm^{-1}, associated to γCH, in-plane ring (phenyl and pyridyl) and CH bendings [33], provide further evidence that the Pr^{3+} ion is coordinated to bath, since they are appreciably red shifted (*vs.* those of free ligand) due to the perturbation induced by the coordination to the lanthanide ion. Other absorptions bands of this complex are those which appear at 2917 cm^{-1} (νC-H), 1650 cm^{-1} (ν_{as}C=C-C=O), 1620 cm^{-1} (ν_{as}C=C-C=O) [33] and 1560 cm^{-1} (νC=O), which are characteristic of the chelated O-bonded fod groups [34,35].
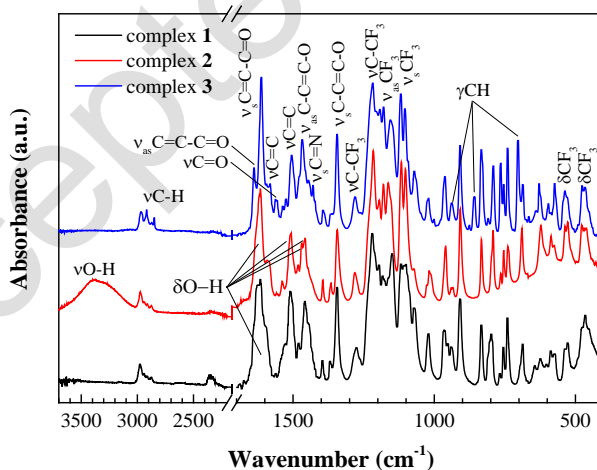

Figure 6. ATR-FTIR spectra of the three complexes.

3.4. *Thermal analysis*

The DSC curve (under N$_2$ atmosphere) shows endothermic effects at 99.6 ℃ and 200.2 ℃ (Figure 7). The endotherms at ca. 100 ℃ and 200 ℃ can be attributed to a transition from crystal to plastic phase and to liquid, respectively. The enthalpies for each transition are 48.5 kJ/mol and 4.7 kJ/mol, respectively.

The TG curve of $[Pr_2(fod)_6(H_2O)\cdot H_2O]$ (also under N_2 atmosphere) shows that the complex is stable up to 100 ºC. At this temperature, a small weight loss (ca. 1%) is observed, which would be compatible with the loss of the solvated water (1 molecule per dimer, ca. 0.9% w). Nevertheless, the decomposition of the complex itself does not take place until 200 ºC: it occurs in a single step and it is complete at 300 ºC (see inset in Figure 7). The weight loss that accompanies this decomposition may correspond to the release of the coordinated water molecule and subsequent loss of the β-diketonate fod ligands.

The stability of the complexes is similar to that of other lanthanide complexes (with Tb^{3+}, Ho^{3+} and Er^{3+}) with the same β-diketonate fod ligand reported by our group [33] and by Irfanullah *et al.* [36,37], but whereas in those complexes the decomposition is due to a volatilization process - which starts at 215 ºC and which is complete at 325-350ºC- in the dimeric Pr^{3+} complex under study the decomposition seems to be favored by the solid to liquid phase transition that -as noted above- occurs at 200.2 ºC.

For complex **2** (not shown), there are three endothermic effects: the peak at 66 ºC can be ascribed to adsorbed methanol evaporation, while those at 160 ºC and 185 ºC are due to consecutive loss of the coordinating ligands. For $[Pr(fod)_3(bath)]$, complex **3** (not shown), there is a single endotherm corresponding to melting at 100.9 ºC, thus displaying a behaviour similar to that of the analogous $[Er(fod)_3(bath)]$ complex [33].
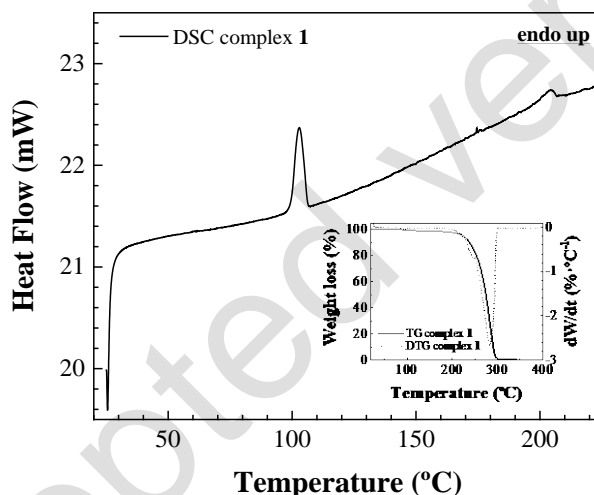

Figure 7. DSC and TG/DTG (*inset*) analysis of $[Pr_2(fod)_6(H_2O)\cdot H_2O]$; $\beta = 10$ °C/min.

3.4.1. *Polarized light thermomicroscopy analysis*

A thermal cycle was followed by polarized light thermomicroscopy analysis. The PLTM images of complex **1** (Figure 8) show rigid solid frontiers up to 190 ºC. The loss of interference colors near 100 ºC shows that a solid-solid transformation to an isotropic phase has taken place. Upon cooling to room temperature the reverse transition does not occur.
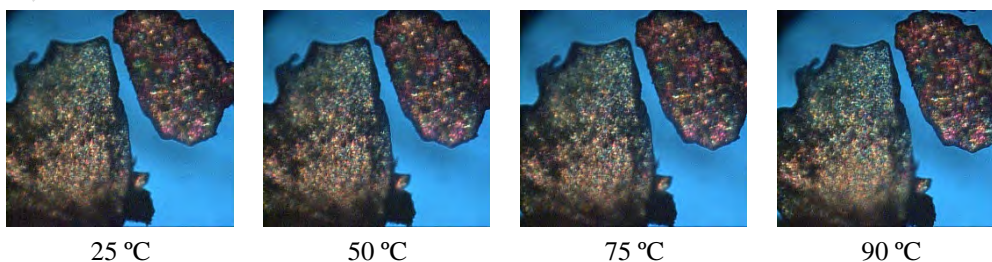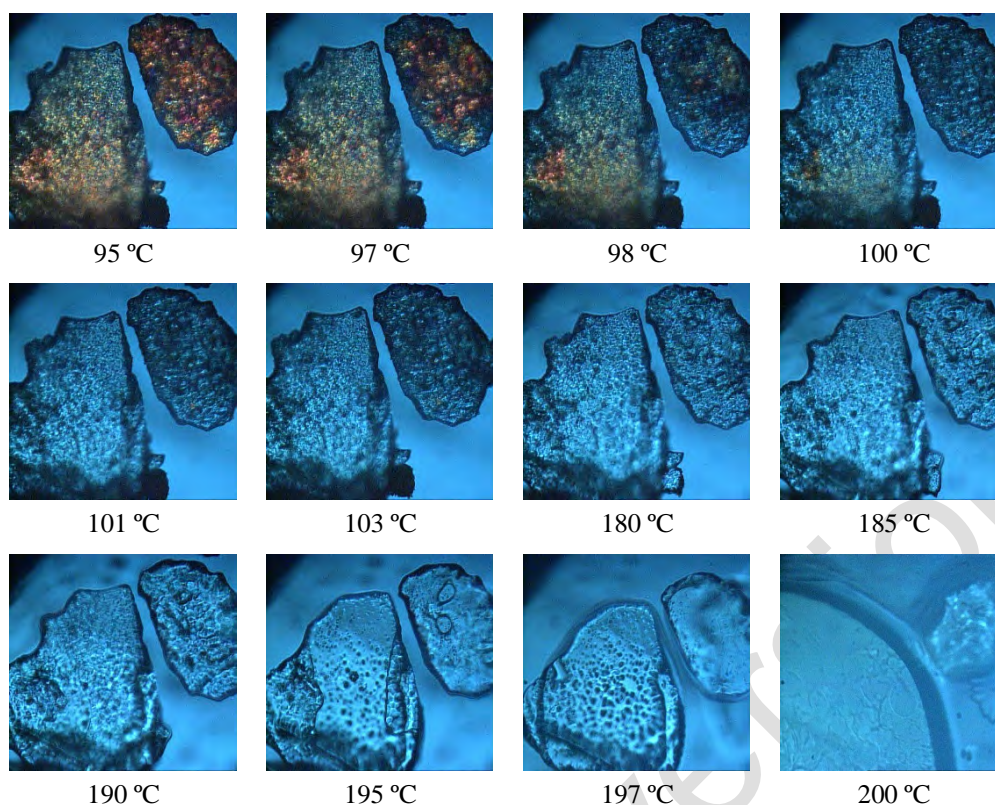

| 25 ºC | 50 ºC | 75 ºC | 90 ºC |

Figure 8. PLTM analysis of $[Pr_2(fod)_6(H_2O)\cdot H_2O]$ sample in the 25 to 200 ℃ range. β = 10 °C/min; magnification 200×.

3.5. *Photophysical properties*

3.5.1. *Absorption and excitation spectra*

The RT spectra derived from absorption and diffuse reflectance measurements in the UV-visible-NIR range (200-1400 nm) for complex **3** (chosen as a representative example of the series) are shown in Figure 9. The broad and intense absorption band in the solid powder measurement (maximum at about 270 nm) can be assigned to electronic intraligand π-π* transitions from the S_0 ground state to the S_1 excited state in the fod moiety [33]. There is a shift in comparison to the UV-Vis (210-800 nm) absorption spectrum recorded in a cyclohexane diluted solution (see the inset in Figure 9), which can be ascribed to the solvent effect: the maximum in this case, also attributable to the π→π* intra-ligand transition in the fod moiety, is at around 290 nm [38-40].

Moreover, sharp peaks associated to intra-configurational 4*f*–4*f* electronic transitions starting from the $^3H_4$ state to $^3P_2$ (~446 nm), $^3P_1$ (~471 nm), $^3P_0$ (~483 nm), $^1D_2$ (~595 nm) and $^1G_4$ (~1010 nm) Pr^{3+} excited levels can be discerned [41].

The excitation spectrum (inset in Figure 9), recorded monitoring the 469 nm emission, displays a broad band (330–420 nm) with maximum at ca. 360 nm, in good agreement with analogous fod complexes [42]. This band corresponds to the excitation of the organic ligands ($S_0 \rightarrow S_1$).
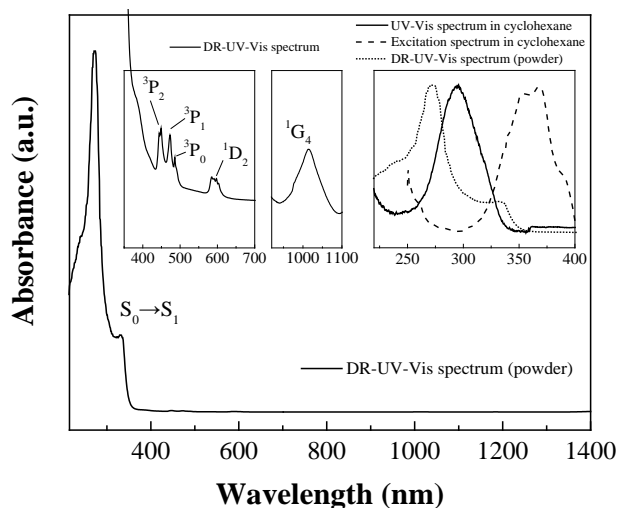
Figure 9. Diffuse reflectance spectrum of complex **3** in the UV–Vis–NIR range at RT. All transitions start from the $^3H_4$ state to the indicated levels. The two insets on the left are zoom-ins (350–700 nm region and 920-1100 nm region) of the DR spectrum. The inset on the right shows a comparison of the DR spectrum *vs.* the UV-Vis spectrum in solution (cyclohexane) and the excitation spectrum (λ_{det}=469 nm).

3.5.2. *PL emission and lifetime measurements*

Upon indirect sensitization of the Pr^{3+} emission by aforementioned *antenna effect* [43,44] (see Figure 11), exciting the ligands at λ_{exc}=370 nm, the three complexes showed different PL behaviors. Complex **3** emitted blue ($\lambda_{max}\approx$490 nm), red ($\lambda_{max}\approx$645 nm) and NIR light ($\lambda_{max}\approx$1004 nm), arising from the $4f$-$4f$ luminescence of Pr^{3+}. Its emission spectrum is shown in Figure 10. The radiative transitions at 490, 610 and 645 nm originate from the upper-lying $^3P_0$-level of Pr^{3+}, while red/infrared emission from $^1D_2$ state is observed at 606 nm and at ca. 1000 nm [15,45]. It should be noted that infrared luminescence of Pr^{3+} at 1060 nm could also be ascribed to the emission from $^1G_4$ level ($^1G_4\rightarrow^3H_4$ transition). However, other authors [15,45,46] have assigned this peak to $^1D_2\rightarrow^3F_4$ emission and in the absence of additional information we will adhere to their conclusion.

The NIR PL decay for the $^1D_2\rightarrow^3F_4$ transition showed a single exponential behavior, with τ=0.07 µs, similar to that attained for other Pr^{3+} complexes with β-diketonates and carboxylates [15,47], and within the range of typically observed luminescence decay times for the NIR transitions in luminescent Pr(III) complexes in solution (from 110 ns to ca. 50 ns) [4]. These lifetimes are much shorter than those of the other near-IR luminescent lanthanides (Yb, Nd, Er) whose emission lifetimes (in aprotic media) are in the µs domain. This may be ascribed to the small gaps between adjacent energy levels which allows particularly efficient non-radiative quenching by vibrations of both ligand and solvent molecules. Nonetheless, it should also be noted that the lifetime value reported herein was recorded in solid state, and it is well know that there is an efficient non-radiative quenching pathway in solid phase samples that leads to shorter lifetimes in the solid compared to the solution phase [4].

Taking into account that the reported radiative (natural) lifetime (τ_{rad}) of Pr^{3+} is 50.7 µs [48], the quantum efficiency of complex **3** may be estimated as [49]: $\Phi_{Ln}=\tau_{obs}/\tau_{rad}$=0.070/50.7=1.38×10^{-3}.

For complexes **1** and **2**, in which H_2O and methanol molecules enter the first coordination sphere, the non-radiative quenching led to lifetime values shorter than the detection limit (25 ns) of the available equipment, and only visible emission was detected (not shown).

The replacement of C–H bonds by C–D bonds, and of O–H vibrations by O–D vibrations may reduce aforementioned radiationless deactivation to a large extent: by replacing H_2O and CH_3OH molecules by D_2O or CD_3OD molecules in analogous complexes, other authors [50,51] confirmed

that it is possible to observe a strong near-infrared luminescence in deuterated solvents. Another strategy would be to resort to a *β*-diketonate with an even longer perfluoroalkyl chain to improve the formation of a hydrophobic shell around the lanthanide ion, so that water molecules cannot coordinate to the central lanthanide ion and cannot quench the luminescence. Nonetheless, this later approach would have limitations: Meshkova *et al.* concluded that, for example, the improvement in luminescence output was small when a C_6F_{13} chain was replaced by an C_8F_{17} chain ([52] and references therein).
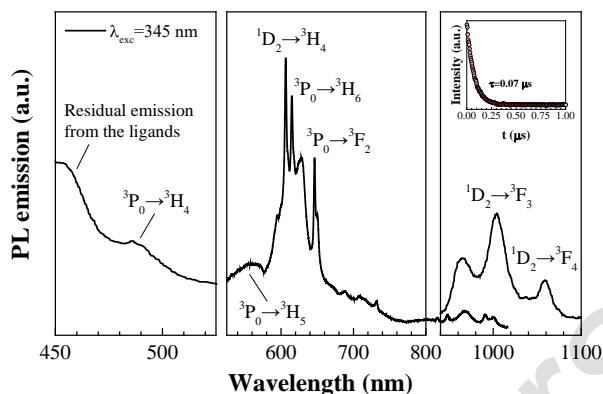

Figure 10. Visible and NIR emission spectra for complex **3** in solution (*left*) and in powder form (*center and right*) upon UV excitation. The PL spectrum is not corrected for the spectral sensitivity of the different detectors and intensities between visible and IR regions cannot be compared. The $^1D_2\rightarrow^3F_4$ luminescence decay curve is shown in the inset on the top right corner.
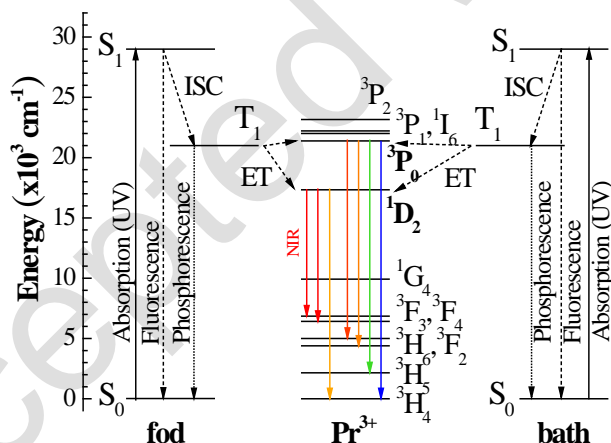

Figure 11. Scheme of the energy transfer mechanism and emission process for complex **3**, depicting the ground-state absorption (GSA), ligand-ligand intersystem crossing (ISC) processes, ligand-to-metal resonant energy transfer (RET) mechanisms, multiphonon de-excitations (---) and PL processes (in color). The singlet and triplet values for fod ($^1\pi\pi^*=35000$ cm^{-1}, $^3\pi\pi^*=22500$ cm^{-1}) and bath ($^1\pi\pi^*=29000$ cm^{-1}, $^3\pi\pi^*=21000$ cm^{-1}) have been taken from the literature [15,53,54].

3.6. *Magnetic behavior*

Variable-temperature magnetic measurements were performed on complex **1** (Figure 12). For complexes **2** and **3**, with only monomers on their crystal structure, the Pr…Pr distances were large enough to preclude any significant magnetic interaction even through superexchange pathways. The presented results include the corrections related to the sample holder and the diamagnetic susceptibility of its components.

For complex **1**, the χT product at room temperature was 5.78 emu·K/mol. In comparison with the expected value for two magnetically non-interacting Pr^{3+} ions (3.20 emu·K/mol) [55], the

experimental value was higher, as expected. The magnetic susceptibility followed the modified Curie-Weiss law: $\chi_M = \chi_0 + C/(T - \theta)$. The suitable parameters were found, with $\chi_0 = 1.14 \times 10^{-2}$ emu·K/mol, Curie constant $C = 2.70$ emu·K/mol and Weiss constant $\theta = -31.42$ K. The effective magnetic moment ($\mu_{eff} = \sqrt{8C}$) is $\mu_{eff} = 4.64 \mu_B$, which is slightly lower than the expected value for a Pr(III) dimer ($4.81 \mu_B$).
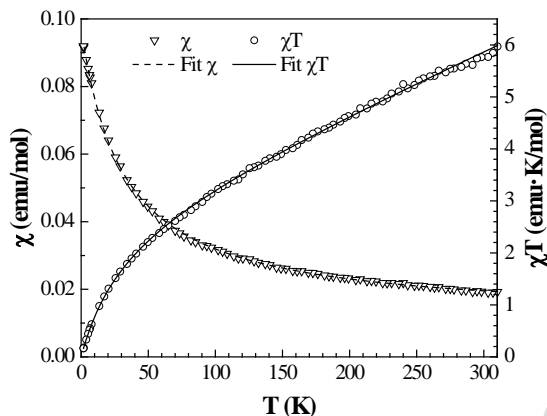

Figure 12. Temperature dependence of the magnetic susceptibility, χ, and χT. Data points have been decimated for clarity reasons.

4. Conclusions

Given the growing interest in low-cost materials based in lanthanides that emit in the near-infrared, three Pr^{3+} coordination complexes with the same highly fluorinated β-diketonate primary sensitizing ligand (Hfod) have been studied. These materials have been thoroughly characterized by X-ray diffraction, FTIR spectroscopy, thermogravimetric analysis, polarized light thermal microscopy, absorption and luminescence spectroscopy in solid state and magnetic measurements.

The homodinuclear complex, $[Pr_2(fod)_6(H_2O)\cdot H_2O]$ displayed antiferromagnetic behavior (precluded in the other two complexes by their larger distances between nearing Pr^{3+} ions) and an infrequent thermal behavior, with an irreversible solid-to-solid transition (at ca. 100 ºC).

With regard to the PL properties, the presence of water and/or methanol molecules in $[Pr_2(fod)_6(H_2O)\cdot H_2O]$ and $[Pr(fod)_3(H_2O)(OHCH_3)]$ led to quenching of the NIR emission by O-H stretching vibrations and only visible emission was observed. Conversely, for the complex in which a diimide completed the first coordination sphere, $[Pr(fod)_3(bath)]$, both visible and NIR emission, arising from $^3P_0$ and $^1D_2$ excited states, was attained (albeit with a short lifetime value for the NIR emission, $\tau = 0.07$ μs). Further work aimed at quenching minimization is under way.

5. Acknowledgements

6. References

[1] Z.Y. Wang, Near-infrared organic materials and emerging applications, CRC Press, Taylor & Francis Group, Boca Raton, FL, USA, 2013, ix, 176 pages pp.

[2] C.-H. Huang, Rare earth coordination chemistry: fundamentals and applications, John Wiley & Sons, Singapore ; Hoboken, NJ, 2010, xxii, 575 p. pp.

[3] M.P. Hehlen, H. Riesen, H.U. Guedel, Synthesis and spectroscopic properties of praseodymium(III) acetate hydrate, Inorg. Chem., 30 (1991) 2273-2277.

[4] G.M. Davies, H. Adams, S.J.A. Pope, S. Faulkner, M.D. Ward, Photophysical properties of Pr(III) and Er(III) complexes of poly(pyrazolyl)borates, Photochemical & Photobiological Sciences, 4 (2005) 829-834.

[5] G.M. Davies, R.J. Aarons, G.R. Motson, J.C. Jeffery, H. Adams, S. Faulkner, M.D. Ward, Structural and near-IR photophysical studies on ternary lanthanide complexes containing poly(pyrazolyl)borate and 1,3-diketonate ligands, Dalton Trans., (2004) 1136-1144.

[6] L. Macalik, J. Hanuza, K. Hermanowicz, W. Oganowski, H. Ban-Oganowska, Emission and absorption properties of the eight-coordinate [Pr(C7H9NO)8](ClO4)3 complex with 3,4-lutidine N-oxide, J. Alloys Compd., 300–301 (2000) 377-382.

[7] L. Macalik, J. Hanuza, K. Hermanowicz, W. Oganowski, H. Ban-Oganowska, Synthesis, chemical characterisation and spectroscopic studies of the six-coordinate 3-halo-2,6-lutidine N-oxide complex [PrCl3(H2O)(BrC7H8NO)2]H2O — a new Pr(III) compound, J. Alloys Compd., 300–301 (2000) 383-388.

[8] M. P. Oude Wolbers, F. C. J. M. van Veggel, B. H. M. Snellink-Ruel, J. W. Hofstraat, F. A. J. Geurts, D. N. Reinhoudt, Photophysical studies of m-terphenyl-sensitized visible and near-infrared emission from organic 1[ratio]1 lanthanide ion complexes in methanol solutions, Journal of the Chemical Society, Perkin Transactions 2, (1998) 2141-2150.

[9] Q. Guo, X.-M. Gao, P. Wang, F.-C. Liu, Hydrothermal syntheses, crystal structures and properties of lanthanide complexes with 4-Hydroxy-6-methylnicotinic acid, J. Mol. Struct., 1024 (2012) 104-109.

[10] C.-H. Li, X.-Z. Song, J.-H. Jiang, H.-W. Gu, L.-M. Tao, P. Yang, X. Li, S.-X. Xiao, F.-H. Yao, W.-Q. Liu, J.-Q. Xie, M.-N. Peng, L. Pan, X.-B. Wu, C. Jiang, S. Wang, M.-F. Xu, Q.-G. Li, Synthesis, crystal structure and thermodynamic properties of a new praseodymium Schiff-base complex, Thermochim. Acta, 581 (2014) 118-122.

[11] I. Pospieszna-Markiewicz, W. Radecka-Paryzek, M. Kubicki, M. Korabik, Z. Hnatejko, Different supramolecular architectures in self-assembled praseodymium(III) and europium(III) complexes with rare coordination pattern of salicylaldimine ligand, Polyhedron, 97 (2015) 167-174.

[12] X.-Q. Song, L. Wang, Q.-F. Zheng, W.-S. Liu, Synthesis, crystal structure and luminescence properties of lanthanide complexes with a new semirigid bridging furfurylsalicylamide ligand, Inorg. Chim. Acta, 391 (2012) 171-178.

[13] X. Zhou, W.-T. Wong, S.C.K. Hau, P.A. Tanner, Structural variations of praseodymium(III) benzoate derivative complexes with dimethylformamide, Polyhedron, 88 (2015) 138-148.

[14] S.B. Meshkova, A.V. Kiriak, Z.M. Topilova, A.M. Andrianov, Praseodymium beta-diketonates and luminescence properties of their solutions, Russian Journal of Inorganic Chemistry, 52 (2007) 556-561.

[15] A.I. Voloshin, N.M. Shavaleev, V.P. Kazakov, Luminescence of praseodymium (III) chelates from two excited states (3P0 and 1D2) and its dependence on ligand triplet state energy, J. Lumin., 93 (2001) 199-204.

[16] A.I. Voloshin, N.M. Shavaleev, V.P. Kazakov, Chemiluminescence of praseodymium (III), neodymium (III) and ytterbium (III) beta-diketonates in solution excited from 1,2-dioxetane decomposition and singlet-singlet energy transfer from ketone to rare-earth beta-diketonates, J. Lumin., 91 (2000) 49-58.

[17] J. Yu, H. Zhang, L. Fu, R. Deng, L. Zhou, H. Li, F. Liu, H. Fu, Synthesis, structure and luminescent properties of a new praseodymium(ɪɪɪ) complex with β-diketone, Inorg. Chem. Commun., 6 (2003) 852-854.

[18] S. Dang, L.N. Sun, S.Y. Song, H.J. Zhang, G.L. Zheng, Y.F. Bi, H.D. Guo, Z.Y. Guo, J. Feng, Syntheses, crystal structures and near-infrared luminescent properties of holmium (Ho) and praseodymium (Pr) ternary complexes, Inorg. Chem. Commun., 11 (2008) 531-534.

[19] M. Irfanullah, K. Iftikhar, The Correlation Between f-f Absorption and Sensitized Visible Light Emission of Luminescent Pr(III) Complexes: Role of Solvents and Ancillary Ligands on Sensitivity, J. Fluoresc., 21 (2011) 673-686.

[20] S. Dang, J. Yu, J.B. Yu, X.F. Wang, L.N. Sun, J. Feng, W.Q. Fan, H.J. Zhang, Novel Holmium (Ho) and Praseodymium (Pr) ternary complexes with fluorinated-ligand and 4,5-diazafluoren-9-one, Mater. Lett., 65 (2011) 1642-1644.

[21] J.P.R. de Villiers, J.C.A. Boeyens, The crystal and molecular structure of the hydrated praseodymium chelate of 1,1,1,2,2,3,3-heptafluoro-7,7-dimethyl-4,6-octanedione, Pr2(fod)6.2H2O, Acta Crystallographica Section B Structural Crystallography and Crystal Chemistry, 27 (1971) 692-702.

[22] G. Sheldrick, SADABS, in, University of Göttingen, Göttingen, Germany, 1996.

[23] G.M. Sheldrick, A short history of SHELX, Acta Crystallogr. Sect. A: Found. Crystallogr., 64 (2007) 112-122.

[24] A.L. Spek, Single-crystal structure validation with the program PLATON, J. Appl. Crystallogr., 36 (2003) 7-13.

[25] R. Sabbah, A. Xu-wu, J.S. Chickos, M.L.P. Leitão, M.V. Roux, L.A. Torres, Reference materials for calorimetry and differential thermal analysis, Thermochim. Acta, 331 (1999) 93-204.

[26] G. Della Gatta, M.J. Richardson, S.M. Sarge, S. Stølen, Standards, calibration, and guidelines in microcalorimetry. Part 2. Calibration standards for differential scanning calorimetry* (IUPAC Technical Report), Pure Appl. Chem., 78 (2006).

[27] W.-y. Yang, L. Chen, S. Wang, Syntheses, Structures, and Luminescence of Novel Lanthanide Complexes of Tripyridylamine, N,N,N'-Tetra(2-pyridyl)-1,4-phenylenediamine and N,N,N',N'-Tetra(2-pyridyl)biphenyl-4,4'-diamine, Inorg. Chem., 40 (2001) 507-515.

[28] P.C. Christidis, I.A. Tossidis, D.G. Paschalidis, L.C. Tzavellas, Tris(acetylacetonato)(1,10-phenanthroline)cerium(III) and Tris(acetylacetonato)(1,10-phenanthroline)praseodymium(III), Acta Crystallographica Section C, 54 (1998) 1233-1236.

[29] T.P. Gerasimova, S.A. Katsyuba, Bipyridine and phenanthroline IR-spectral bands as indicators of metal spin state in hexacoordinated complexes of Fe(II), Ni(II) and Co(II), Dalton Trans., 42 (2013) 1787.

[30] S.F. Tayyari, M. Vakili, A.-R. Nekoei, H. Rahemi, Y.A. Wang, Vibrational assignment and structure of trifluorobenzoylacetone, Spectrochim. Acta, Pt. A: Mol. Biomol. Spectrosc., 66 (2007) 626-636.

[31] M. Ristić, S. Popović, S. Musić, Formation of Oxide Phases in the System Pr-Fe-O, Croat. Chem. Acta, 86 (2013) 281-285.

[32] B.C. Smith, Infrared spectral interpretation : a systematic approach, CRC Press, Boca Raton, 1999, 265 p. pp.

[33] P. Martín-Ramos, M. Ramos Silva, F. Lahoz, I.R. Martín, P. Chamorro-Posada, M.E.S. Eusebio, V. Lavín, J. Martín-Gil, Highly fluorinated erbium(III) complexes for emission in the C-band, J. Photochem. Photobiol. A: Chem., 292 (2014) 16-25.

[34] S. Pinchas, B.L. Silver, I. Laulicht, Infrared Absorption Spectra of the 18O-Labeled Acetylacetonates of Cr(III) and Mn(III), The Journal of Chemical Physics, 46 (1967) 1506-1510.

[35] A.K. Gupta, R.K. Poddar, Improved synthesis and reactivity of tris(acetylacetonato) ruthenium (III), Indian Journal of Chemistry Section A, 39 (2000) 457-460.

[36] M. Irfanullah, K. Iftikhar, New hetero-dilanthanide complexes containing Ln1(fod)3 and Ln2(fod)3 fragments (Ln=Pr–Nd; Nd–Sm; Eu–Tb and Ho–Er) linked by bis-diimine bridging ligand, Inorg. Chem. Commun., 13 (2010) 694-698.

[37] M. Irfanullah, K. Iftikhar, New dinuclear lanthanide(III) complexes based on 6,6,7,7,8,8,8-heptafluoro-2,2-dimethyl-3,5-octanedione and 2,2′-bipyrimidine, Inorg. Chem. Commun., 12 (2009) 296-299.

[38] L.S. Villata, E. Wolcan, M.R. Féliz, A.L. Capparelli, Solvent quenching of the 5D0 → 7F2 emission of Eu(6,6,7,7,8,8,8-heptafluoro-2,2-dimethyl-3,5-octanedionate)3, J. Photochem. Photobiol. A: Chem., 115 (1998) 185-189.

[39] V.I. Gerasimova, Optical Spectroscopy of the Eu(FOD)₃ Complex Impregnated into the Free Volume of Nanoporous Glass and Polymethylmethacrylate Using Supercritical Carbon Dioxide, Opt. Spectrosc., 98 (2005) 564.

[40] V.I. Gerasimova, Y.S. Zavorotny, A.O. Rybaltovskii, A.A. Antoshkov, V.I. Sokolov, E.V. Troitskaya, V.N. Bagratashvili, Modification of the optical properties of fluoropolymers by supercritical fluid impregnation with europium β-diketonates, Russian Journal of Physical Chemistry B, 4 (2011) 1149-1157.

[41] B. Keller, J. Legendziewicz, J. Gliński, S. Samela, Investigation of the optical and ultrasonic properties of praseodymium and cerium chlorides in nonaqueous solutions, J. Alloys Compd., 300–301 (2000) 334-340.

[42] M. Irfanullah, K. Iftikhar, A comparative study of 1H NMR and sensitized visible light emission of an extended series of dinuclear lanthanide complexes, J. Photochem. Photobiol. A: Chem., 224 (2011) 91-101.

[43] N. Sabbatini, M. Guardigli, J.-M. Lehn, Luminescent lanthanide complexes as photochemical supramolecular devices, Coord. Chem. Rev., 123 (1993) 201-228.

[44] G.F. de Sá, O.L. Malta, C. de Mello Donegá, A.M. Simas, R.L. Longo, P.A. Santa-Cruz, E.F. da Silva, Spectroscopic properties and design of highly luminescent lanthanide coordination complexes, Coord. Chem. Rev., 196 (2000) 165-195.

[45] Z. Hong, C. Liang, R. Li, F. Zang, D. Fan, W. Li, L.S. Hung, S.T. Lee, Infrared and visible emission from organic electroluminescent devices based on praseodymium complex, Appl. Phys. Lett., 79 (2001) 1942.

[46] E.B. Sveshnikova, N.T. Timofeev, Opt. Spectrosc., 48 (1980) 276

[47] M.A. Katkova, A.G. Vitukhnovsky, M.N. Bochkarev, Coordination compounds of rare-earth metals with organic ligands for electroluminescent diodes, Russian Chemical Reviews, 74 (2005) 1089-1109.

[48] M.J. Weber, Radiative and Multiphonon Relaxation of Rare-Earth Ions in ${\mathrm{Y}}_{2}$${\mathrm{O}}_{3}$, Phys. Rev., 171 (1968) 283-291.

[49] J.-C.G. Bünzli, S.V. Eliseeva, Basics of Lanthanide Photophysics, in: P. Hänninen, H. Härmä (Eds.) Lanthanide Luminescence: Photophysical, Analytical and Biological Aspects, Springer Berlin Heidelberg, Berlin, Heidelberg, 2011, pp. 1-45.

[50] Y. Hasegawa, K. Murakoshi, Y. Wada, S. Yanagida, J.-H. Kim, N. Nakashima, T. Yamanaka, Enhancement of luminescence of Nd3+ complexes with deuterated hexafluoroacetylacetonato ligands in organic solvent, Chem. Phys. Lett., 248 (1996) 8-12.

[51] S. Yanagida, Y. Hasegawa, Y. Wada, Remarkable luminescence of novel Nd(III) complexes with low-vibrational hexafluoroacetylacetone and DMSO-d6 molecules, J. Lumin., 87-89 (2000) 995-998.

[52] K. Binnemans, Rare-earth beta-diketonates, in: K.A. Gschneidner, J.-C.G. Bünzli, V.K. Pecharsky (Eds.) Handbook on the Physics and Chemistry of Rare Earths, Elsevier B.V., North-Holland, 2005, pp. 107-272.

[53] D.B. Ambili Raj, S. Biju, M.L.P. Reddy, One-, Two-, and Three-Dimensional Arrays of Eu3+-4,4,5,5,5-pentafluoro-1-(naphthalen-2-yl)pentane-1,3-dione complexes: Synthesis, Crystal Structure and Photophysical Properties, Inorg. Chem., 47 (2008) 8091-8100.

[54] D.B. Ambili Raj, S. Biju, M.L.P. Reddy, Highly luminescent europium(III) complexes containing organosilyl 4,4,5,5,5-pentafluoro-1-(naphthalen-2-yl)pentane-1,3-dionate ligands grafted on silica nanoparticles, J. Mater. Chem., 19 (2009) 7976-7983.

[55] J. Vallejo, J. Cano, I. Castro, M. Julve, F. Lloret, O. Fabelo, L. Cañadillas-Delgado, E. Pardo, Slow magnetic relaxation in carbonato-bridged dinuclear lanthanide(iii) complexes with 2,3-quinoxalinediolate ligands, Chem. Commun., 48 (2012) 7726.